

# p38 $\gamma$ MAPK contributes to left ventricular remodeling after pathologic stress and disinhibits calpain through phosphorylation of calpastatin

Aminah A. Loonat,\* E. Denise Martin,\* Negin Sarafraz-Shekary,\* Katharina Tilgner,\* Nicholas T. Hertz,<sup>†</sup> Rebecca Levin,<sup>†</sup> Kevan M. Shokat,<sup>†</sup> Alma L. Burlingame,<sup>†</sup> Pelin Arabacilar,\* Shahzan Uddin,\* Max Thomas,\* Michael S. Marber,\* and James E. Clark\*<sup>1</sup>

\*School of Cardiovascular Medicine and Science, British Heart Foundation (BHF) Centre, King's College London, London, United Kingdom; and <sup>†</sup>University of California–San Francisco, San Francisco, California, USA

**ABSTRACT:** Despite the high and preferential expression of p38 $\gamma$  MAPK in the myocardium, little is known about its function in the heart. The aim of the current study was to elucidate the physiologic and biochemical roles of p38 $\gamma$  in the heart. Expression and subcellular localization of p38 isoforms was determined in mouse hearts. Comparisons of the cardiac function and structure of wild-type and p38 $\gamma$  knockout (KO) mice at baseline and after abdominal aortic banding demonstrated that KO mice developed less ventricular hypertrophy and that contractile function is better preserved. To identify potential substrates of p38 $\gamma$ , we generated an analog-sensitive mutant to affinity tag endogenous myocardial proteins. Among other proteins, this technique identified calpastatin as a direct p38 $\gamma$  substrate. Moreover, phosphorylation of calpastatin by p38 $\gamma$  impaired its ability to inhibit the protease, calpain. We have identified p38 $\gamma$  as an important determinant of the progression of pathologic cardiac hypertrophy after aortic banding in mice. In addition, we have identified calpastatin, among other substrates, as a novel direct target of p38 $\gamma$  that may contribute to the protection observed in p38 $\gamma$ KO mice.—Loonat, A. A., Martin, E. D., Sarafraz-Shekary, N., Tilgner, K., Hertz, N. T., Levin, R., Shokat, K. M., Burlingame, A. L., Arabacilar, P., Uddin, S., Thomas, M., Marber, M. S., Clark, J. E. p38 $\gamma$  MAPK contributes to left ventricular remodeling after pathologic stress and disinhibits calpain through phosphorylation of calpastatin. *FASEB J.* 33, 13131–13144 (2019). www.fasebj.org

**KEY WORDS:** heart · hypertrophy · failure · protection · kinase

The current study provides experimental evidence for a putative role for p38 $\gamma$  MAPK in the progression of cardiac hypertrophy and heart failure and elucidates a mechanism of action. By using an *in vivo* mouse model of cardiac hypertrophy, this study demonstrates how ablation of p38 $\gamma$  MAPK expression ameliorates cardiac function after aortic constriction. By using a modified analog-sensitive kinase *in vitro* and subsequent proteomic analysis, we identify

putative substrates of p38 $\gamma$  MAPK and demonstrate the functional consequence of substrate phosphorylation.

p38 MAPKs are stress-activated serine/threonine kinases that sense a variety of cardiac pathologies (1). The family consists of 4 isoforms— $\alpha$ ,  $\beta$ ,  $\gamma$ , and  $\delta$ . Studies have historically focused on the p38 $\alpha$  and p38 $\beta$  isoforms as they are ubiquitously expressed and inhibited by widely available tools, including pyridinylimadazole inhibitors, such as SB203580. The remaining 2 p38 MAPK isoforms are not inhibited by pyridinylimadazoles and exhibit differential expression patterns (2). For example, p38 $\gamma$  is highly expressed in skeletal and cardiac muscle, and p38 $\delta$  is highly expressed in endocrine glands (3).

Whereas all 4 isoforms are expressed in the heart, p38 $\alpha$  and p38 $\gamma$  have been shown to be the 2 most abundantly expressed isoforms, with comparable myocardial protein content (3). There are extensive studies that have documented the role of p38 $\alpha$  in various cardiac disease states, especially in response to ischemia and infarction (1); however, little has been reported about the functional role of p38 $\gamma$  in the heart. Given the differential localization of p38 $\alpha$  and p38 $\gamma$  in unstimulated cardiomyocytes and in

**ABBREVIATIONS:** AS, analog sensitive; CID, collision-induced dissociation; IPTG, isopropyl  $\beta$ -D-1-thiogalactopyranoside; KO, knockout; LC-MS/MS, liquid chromatography–tandem mass spectrometry; LV, left ventricle; NFAT, nuclear factor of activated T cell; PNBM, p-nitrobenzyl mesylate; WT, wild type;  $\beta$ -MHC,  $\beta$ -myosin heavy chain

<sup>1</sup> Correspondence: School of Cardiovascular Medicine and Sciences, The BHF Centre, The Rayne Institute, King's College London, 4th Floor Lambeth Wing, St. Thomas' Hospital, Lambeth Palace Rd., London SE1 7EH, United Kingdom. E-mail: james.2.clark@kcl.ac.uk

This is an Open Access article distributed under the terms of the Creative Commons Attribution 4.0 International (CC BY 4.0) (<http://creativecommons.org/licenses/by/4.0/>) which permits unrestricted use, distribution, and reproduction in any medium, provided the original work is properly cited.

doi: 10.1096/fj.201701545R

This article includes supplemental data. Please visit <http://www.fasebj.org> to obtain this information.

hearts of mice subjected to pressure overload (3, 4), it is unlikely that p38 $\gamma$  is functionally redundant.

The lack of tool compounds has also impeded the identification of p38 $\gamma$  substrates. The PDZ domain-interacting motif—exclusive to p38 $\gamma$  among the MAPK family—has aided in the search for specific substrates (5). The short amino acid sequence, KETAL, in the C-terminal of p38 $\gamma$  can directly dock to PDZ domains of proteins and therefore adds a unique dimension to p38 $\gamma$  signaling. Examples of proteins that have been found to interact with p38 $\gamma$  *via* their PDZ domains and undergo phosphorylation are  $\alpha$ 1-syntrophin (5), PSD-95 (6), SAP97 (7), PTPH1 (8), and DEPTOR (9); however, there are likely to be cardiac substrates of p38 $\gamma$  that are not PDZ dependent. One technique to identify such substrates is an *in vitro* chemical genetic approach first described by Shokat and colleagues (10). This technique was initially developed to identify substrates of v-Src tyrosine kinase. The approach requires the generation of an analog-sensitive (AS) kinase that can utilize bulky, orthogonal N<sup>6</sup> expanded ATP analogs that cannot be used by wild-type (WT) kinases. The ATP analog is also modified at the  $\gamma$ -phosphate to substitute a thiol group in place of the hydroxyl group (11). As such, substrate proteins undergo thiophosphorylation, which allows substrates of the kinase of interest to be specifically tracked and identified from a complex mixture of proteins, such as cell or tissue extracts.

The aim of the current study was to examine the role that p38 $\gamma$  plays cardiac hypertrophy by using gene-targeted mouse lines and to identify its potential myocardial substrates *via* a Shokat approach.

## MATERIALS AND METHODS

### Mice colonies

All animal experiments were carried out in accordance with Home Office regulations as detailed in the Home Office Guidance on the Operation of Animals (Scientific Procedures) Act 1986 HMSO (London), which mirrors those of the *Guide for the Care and Use of Laboratory Animals* [National Institutes of Health (NIH), Bethesda, MD, USA]. We used mice with targeted disruption of p38 $\gamma$  and p38 $\delta$  MAPK (p38 $\gamma$  $\delta$ KO), the generation of which has been described by Sabio *et al.* (7). These mice were backcrossed with outbred C57/BL6 mice for at least 5 generations to develop p38 $\gamma$  single knockout (KO) mice (p38 $\gamma$ KO). PCR protocols for genotyping these mice have been described by Sabio *et al.* (7).

### Abdominal aortic banding

Male mice (age 8–10 wk, 22–26 g) from p38 $\gamma$  $\delta$ KO or p38 $\gamma$ KO colonies were used in all experiments. Mice were subjected to abdominal aortic banding as described by Boguslavskiy *et al.* (12). In brief, a small metal tube (28 G) was tied against the supra-renal aorta to restrict blood flow and provide increased afterload and a reproducible decrease in renal blood flow to induce cardiac hypertrophy. Buprenorphine (single-dose 20  $\mu$ g/kg, *i.p.*; Vetergesic, Ceva Animal Health Ltd., France) was used for perioperative analgesia. After invasive pressure–volume measurements, euthanasia was performed with an overdose of 300 mg/kg pentobarbital (Pentoject). Death was confirmed by monitoring cardiac activity and respiration. For immunohistochemistry, heart excision was performed after terminal anesthesia by intraperitoneal injection of pentobarbital (300 mg/kg) and heparin (150 IU) and flushing of the heart using ice-cold saline.

After excision, hearts were coated in optimum cutting temperature compound (TissueTek; Sakura, Torrance, CA, USA) and snap-frozen in a bath of liquid nitrogen-cooled isopentane and attached to a cork board before cryosectioning at 30  $\mu$ m.

### Echocardiography and left ventricle function

All mice received preoperative cardiac ultrasound, and serial echocardiography was used to assess cardiac function after surgery. Mice were anesthetized by using 2% isoflurane (100% oxygen), maintained on a homeothermic platform, and examined by echocardiography using a high-resolution Vevo 770 echocardiography system (VisualSonics, Toronto, ON, Canada) with an RMV-707B transducer at 30 MHz. High-resolution parasternal left ventricle (LV) long- and short-axis M-mode and B-mode images were obtained for offline measurements with Vevo software (VisualSonics) to calculate LV function and mass. At the end of experiments, mice were subjected to invasive LV function assessment by pressure–volume analysis as described by Clark *et al.* (13).

### Immunocytochemistry

Mouse cardiac myocytes were isolated as described by Haworth *et al.* (14). Freshly isolated cardiac myocytes were cultured on laminin-coated culture dishes for 1 h in DMEM (MilliporeSigma, St. Louis, MO, USA). Media were removed and cells were washed with PBS and fixed by 4% paraformaldehyde in PBS for 15 min. This was followed by three 5-min washes with PBS. Cells were next permeabilized with 0.2% Triton X-100 in PBS, followed by a 5-min wash with PBS and blocking with 100  $\mu$ l/dish of 5% normal goat serum. Specific Abs against pan-isoform p38 (9212; Cell Signaling Technology, Danvers, MA, USA), p38 $\beta$  (P38-11A5; Thermo Fisher Scientific, Waltham, MA, USA), p38 $\gamma$  (AF1347; R&D Systems, Minneapolis, MN, USA), and p38 $\delta$  (ab188324; Abcam, Cambridge, United Kingdom) were diluted 1:100 in addition to either primary mouse  $\alpha$ -actinin (diluted 1:500) or primary rabbit  $\alpha$ -actinin (diluted 1:200) in buffer that contained 20 mM Tris base, 155 mM NaCl, 2 mM EGTA, 2 mM MgCl<sub>2</sub>, pH 7.5, and 1% bovine serum albumin. Dishes were placed into a humid chamber and incubated overnight at 4°C. The next day, cells were washed in PBS and incubated overnight at 4°C with secondary Abs: donkey anti-mouse Cy3 (diluted 1:500; 715-165-150; Jackson ImmunoResearch Labs, West Grove, PA, USA), goat anti-rabbit Alexa Fluor 647 (diluted 1:100; 111-605-003; Jackson ImmunoResearch Labs), and DAPI (diluted 1:100; MilliporeSigma). Cells were then washed as before and mounted with a droplet of mounting medium (0.1 M Tris, 35 ml glycerol, and 2.5 g *n*-propyl gallate) and covered with 30-mm-diameter glass coverslips (Science Warehouse, Leeds, United Kingdom). The vertical sides of each dish were removed with a hot wire and coverslips were sealed with nail varnish. Each dish was then glued onto a microscope slide and kept at 4°C until analysis by confocal microscopy.

### Immunohistochemistry

After being cryosectioned and mounted onto poly-lysine slides (Polysine; VWR, Radnor, PA, USA), tissue sections were air dried and briefly fixed with 100% acetone for 15 min at room temperature. Heart sections were circled with wax pen (Dako, Carpinteria, CA, USA), then incubated with PBS that contained 0.1% (*v/v*) Triton X-100 and 1% (*w/v*) bovine serum albumin for 20 min. Samples were incubated overnight at 4°C with specific primary Abs against  $\beta$ -myosin heavy chain ( $\beta$ -MHC; diluted 1:200 in  $\beta$ -PBS; MilliporeSigma). The next day, samples were washed with PBS and incubated for an additional 2 h with secondary Ab (diluted 1:200 in PBS and Cy3-conjugated donkey anti-mouse IgG; 715-165-150; Jackson ImmunoResearch Labs) and Alexa Fluor 488-conjugated wheat germ agglutinin (Thermo Fisher Scientific). Slides were

washed and coverslips were placed with mounting medium that contained DAPI (Dako) before being visualized at the appropriate wavelengths by using a Leica SP-5 confocal microscope (Leica Microsystems, Wetzlar, Germany). A total of 5 images from each heart section were used to quantify myocyte cross-sectional area by using a custom macro in ImageJ (v1.50i; NIH), with at least 250 cells being measured for each heart.  $\beta$ -MHC was scored independently as positive (red) cells per high-powered field.

### Cloning and purification of recombinant p38 $\gamma$ proteins

The clone of the open reading frame of murine *mapk12* (p38 $\gamma$ ) was a kind gift from the Rudnicki Laboratory (University of Ottawa, Ottawa, ON, Canada) (15). The full-length insert was subcloned into pETDuet-1 (Thermo Fisher Scientific) 3' to a 6 $\times$  His coding sequence. Insertion of cDNA into pETDuet-1 was confirmed by electrophoresis on agarose gels and sequencing. For generating C' truncated p38 $\gamma$  and AS p38 $\gamma$ , mutations were introduced by using the QuikChange II Site-Directed Mutagenesis Kit (Agilent Technologies, Santa Clara, CA, USA) according to the manufacturer's instructions. For generating AS p38 $\gamma$ , the gatekeeper methionine 109 residue was mutated to a glycine and additional rescue mutations—A160L and L170A—were introduced to prevent the loss of kinase activity. Mutagenesis was confirmed by sequencing. p38 $\gamma$  constructs were transformed into the *Escherichia coli*-competent strain, Rosetta BL21 (DE3; Biotline, Toronto, ON, Canada). Transformed *E. coli* were then selected on LB agar medium that contained 100  $\mu$ g/ml ampicillin. Transformed bacteria were inoculated in LB media that contained 100  $\mu$ g/ml ampicillin and grown to an optical density of 0.5 at 600 nm, then expression of 6 $\times$  His protein was induced by the addition of 1 mM isopropyl- $\beta$ -D-thiogalactoside (IPTG) for 5 h at 21°C with constant shaking. p38 $\gamma$  proteins (6 $\times$  His) were purified by immobilized metal affinity chromatography using nickel-nitriloacetic acid agarose beads (Qiagen, Germantown, MD, USA) and a batch protocol as follows: bacterial cell pellets were resuspended in ice-cold lysis buffer (50 mM Tris, pH 7.4, 500 mM NaCl, 2 mM DTT, and 10 mM imidazole that contained a protease inhibitor cocktail; Roche, Basel, Switzerland). Cell lysis was performed by using a high-intensity ultrasonic processor. Lysates were clarified by centrifugation at 10,000 rpm for 30 min at 4°C. Supernatants were filtered through 0.45- $\mu$ m membrane filters before being incubated with lysis buffer–equilibrated nickel-nitriloacetic acid agarose beads for 1 h at 4°C on a rotator. Beads were pelleted by centrifugation at 3000 rpm for 5 min at 4°C and the supernatant was discarded. Beads were subsequently washed 6 times with 15 ml ice-cold wash buffer (50 mM Tris, pH 7.4, 500 mM NaCl, 2 mM DTT, and 20 mM imidazole). p38 $\gamma$  proteins (6 $\times$  His) were eluted by increasing the imidazole concentration stepwise from 0.05 to 0.5 M. p38 $\gamma$  6 $\times$  His peak fractions were pooled and dialyzed overnight at 4°C against 2  $\times$  2 L of a buffer that consisted of 50 mM Tris, pH 7.4, 100 mM NaCl, and 2 mM DTT. The purity of 6 $\times$  His p38 $\gamma$  proteins was further refined by ion exchange chromatography on a MonoQ 5/10 column (GE Healthcare Lifesciences, Little Chalfont, United Kingdom) equilibrated in 50 mM Tris, pH 7.4, 100 mM NaCl, and 2 mM DTT. p38 $\gamma$  protein was eluted by applying 40 column volumes of a linear 0.1–0.6 M NaCl gradient. p38 $\gamma$  eluted at  $\sim$ 190 mM NaCl. All chromatographic steps were performed at 4°C. Fractions from each chromatographic step were analyzed by SDS-PAGE and/or Western blot analysis. Fractions that contained highly purified p38 $\gamma$  protein were pooled and used for subsequent biochemical studies. Protein concentration was determined by Pierce Bradford assay (Thermo Fisher Scientific).

### Activation of nonactive p38 $\gamma$ proteins

Purified nonactive 6 $\times$  His p38 $\gamma$  proteins (0.2 mg/ml) were activated by incubation with constitutively active MBP–MAPK

kinase 6 (0.02 mg/ml) in the presence of 0.1 mM ATP and 1 $\times$  kinase buffer (50 mM Tris, pH 7.5, 10 mM MgAc, 0.1 mM EGTA, 0.1% 2-ME) for 1.5 h at 30°C without mixing. To separate MAPK kinase 6 from p38 $\gamma$  proteins, kinase reactions were incubated with amylose resin for 30 min at 4°C. Resin was pelleted by centrifugation at 3000 rpm for 5 min at 4°C, and the supernatant that contained activated protein was collected and analyzed for phosphorylation by SDS-PAGE, Phostag SDS-PAGE, and Western blot analysis. Activated proteins were dialyzed into storage buffer (50 mM Tris, pH 7.5, 0.1 mM EGTA, 270 mM sucrose, 150 mM NaCl, 0.1% 2-ME, 0.2 mM PMSF, and 1 mM benzamide) overnight at 4°C.

### HEK cell transfection

HEK293 cells were transfected at 70% confluency in Opti-MEM I (Thermo Fisher Scientific) by using Turbofect (Thermo Fisher Scientific) with WT or canonically mutated TAB1 (V408A, M409A; 1-418B; CM) TAB1 plasmid DNA as described by DeNicola *et al.* (16).

### Cloning and purification of recombinant LDB3 protein

His-LDB3 was generated by subcloning the open reading frame of murine *ldb3* from the pcR4-TOPO vector (Source Bioscience, Nottingham, United Kingdom) into the pETDuet-1 (Thermo Fisher Scientific) expression vector (Novagen, London, United Kingdom). Subsequent LDB3 cloning and purification steps were as described above for the generation of recombinant p38 $\gamma$  proteins with the following modification: bacteria were cultured at 26°C after IPTG induction.

### Cloning and purification of recombinant calpastatin proteins

RNA was extracted from WT mouse heart stored in RNAlater (Thermo Fisher Scientific) by using an RNeasy Fibrous Tissue Kit (Qiagen) according to the manufacturer's instructions. cDNA was generated by using Superscript III Reverse Transcriptase (Thermo Fisher Scientific) according to the manufacturer's instructions. The resulting RNA/cDNA hybrids were used as templates to generate double-stranded calpastatin DNA using Platinum Pfx DNA polymerase (Thermo Fisher Scientific) according to the manufacturer's instructions. The full-length insert was subcloned into pGEX-3X (GE Healthcare Lifesciences) 3' to a GST coding sequence. Insertion of cDNA into pGEX-3X was confirmed by electrophoresis on agarose gels and sequencing. To generate calpastatin mutants, mutations were introduced by using the QuikChange II Site-Directed Mutagenesis Kit according to the manufacturer's instructions. Mutagenesis was confirmed by sequencing. Transformation and expression of WT and mutant calpastatin constructs into *E. coli* were carried out as described for p38 $\gamma$  with the following variations: 0.1 mM IPTG was used to induce the expression of calpastatin proteins; and bacterial cells were grown at 37°C after induction. GST-calpastatin proteins were purified by glutathione sepharose chromatography.

Bacterial cells were resuspended in ice-cold lysis buffer (PBS, pH 7.4, 2 mM DTT, and protease inhibitor cocktail; Roche). Cell lysis was performed by using a high-intensity ultrasonic processor. Lysates were clarified by centrifugation at 4600 rpm for 40 min at 4°C. Supernatant was filtered through a 0.45- $\mu$ m membrane filter before being incubated with lysis buffer–equilibrated glutathione sepharose beads (GE Healthcare Lifesciences) for 1 h at 4°C on a rotator. Beads were pelleted by centrifugation at 3000 rpm for 1 min at 4°C and the supernatant was discarded. Beads were subsequently washed with 10 ml ice-cold PBS for 2 min at room temperature on a rotator. We carried out 5 additional 10-ml

washes. GST-calpastatin was eluted by applying 1.5-ml volumes of a 10–40 mM reduced glutathione gradient. Fractions that contained GST-calpastatin were pooled and dialyzed overnight at 4°C against 2 × 2 L of buffer that contained 50 mM Tris, pH 8.0, 50 mM NaCl, 2 mM DTT.

### **In vitro kinase assays**

Phosphorylation of substrates was performed *in vitro* in kinase buffer (25 mM Tris, pH 7.5, 5 mM β-glycerophosphate, 2 mM DTT, 0.2 mM Na<sub>3</sub>VO<sub>4</sub>, and 10 mM MgCl<sub>2</sub>) and contained 200 ng of active p38γ, 1 mM ATP, ATP-γ-S or 6-PhEt-ATPγS (BioLog, Minden, Germany), and 1 μg of recombinant ATF2 (Cell Signaling Technology), α1-syntrophin (Creative Biomart, Shirley, NY, USA), LDB3, or calpastatin substrate. Reactions were incubated at 30°C for 30 min. Reactions were stopped by adding 2× Laemmli sample buffer and boiling at 100°C for 5 min. To detect thiophosphorylated substrates, kinase reactions were stopped with 20 mM EDTA and alkylated with 5 mM p-nitrobenzyl mesylate (PNBM; Abcam) or vehicle for 1–2 h at room temperature before the addition of 2× Laemmli sample buffer.

### **Thiophosphorylation of p38γ substrates in heart homogenate**

Kinase reactions (220 μl) were performed as above but contained 2 mg of heart homogenate, 20 μg of active p38γ, 1 mM Phe-Eth-γ-S, 0.4 mM ATP, and 3 mM GTP. Reactions were incubated at 30°C for 1 h and stopped with 20 mM EDTA. A 10-μl sample of each reaction was removed for alkylation with 5 mM PNBM to check the reaction by Western blot analysis using an anti-thiophosphate ester Ab. Samples were frozen in liquid N<sub>2</sub> and stored at –80°C until the covalent capture procedure was performed.

### **Immunoblot analysis**

Samples were resolved on a 10% reducing SDS polyacrylamide gel and blotted onto a PVDF membrane. Membranes were blocked for 1 h in 1.33% low-fat milk and 0.33% bovine serum albumin in Tris-buffered saline (pH 7.4) and 0.1% Tween-20. Primary Abs were incubated overnight at 4°C with agitation. Abs used included anti-dual-phosphorylated p38 (Thr180 and Tyr182; 4511; Cell Signaling Technology), anti-p38α (1:2000; MA5-15116; Thermo Fisher Scientific), anti-p38β (1:1000; P38-11A5; Thermo Fisher Scientific), anti-p38δ (1:2000; ab188324; Abcam), anti-p38γ (1:8000; AF1347; R&D Systems), anti-phosphorylated ATF2 (1:5000; 9221; Cell Signaling Technology), anti-ATF2 (1:4000; 9226; Cell Signaling Technology), anti-thiophosphate ester (1:8000; ab92570; Abcam), anti-PDLIM5 (H00010611-A02; Abnova, Taipei, Taiwan), anti-α1-syntrophin (ab11187; Abcam), anti-calpastatin (1:2000; 4146; Cell Signaling Technology), custom anti-dual-phosphorylated calpastatin (T197/S200), and anti-phosphorylated calpastatin (1:1000; T448; Cambridge Research Biochemicals, Billingham, United Kingdom). After washing and incubating with the appropriate horseradish peroxidase-conjugated secondary Ab (GE Healthcare Lifesciences), Ab-antigen complexes were visualized by ECL (Pierce, Rockford, IL, USA).

### **Estimation of p38 MAPK isoform expression**

Whole-heart homogenates were spiked with GST-tagged recombinant proteins (240 ng/well) (Cell Signaling Biotechnology) and probed with isoform-specific mAbs and a total (pan-isoform) Ab as described above. In this way, by using serially diluted recombinant

protein (0.4–246.0 mg/well), standard curves were generated for each specific isoform Ab, and the relative endogenous expression of each isoform was determined by using GraphPad Prism (v6; GraphPad Software, La Jolla, CA, USA).

### **Phostag SDS-PAGE and silver staining**

For Phostag gel analysis of calpastatin phosphorylation, a Bis-Tris-buffered neutral pH gel system was adopted. For this system, samples were added to 2× lithium dodecyl sulfate loading buffer (282 mM Tris base, 212 mM Tris HCl, pH 8.5, 20% glycerol, 4% lithium dodecyl sulfate, 200 μM DTT, 1 mM EDTA, 0.66 mM SERVA Blue G250, and 0.35 mM Phenol Red) to give a 1× final concentration. Samples were heated to 70°C for 10 min and centrifuged at 10,000 rpm for 2 min. Samples were separated by hand-cast 8% Bis-Tris PAGE mini-gels that were supplemented with 50 μM Phostag acrylamide and 100 μM Zn(NO<sub>3</sub>)<sub>2</sub> with a 4% stacking gel. Gels were electrophoresed at 90 V *via* the stacking gel for ~20 min and 120 V *via* the resolving gel. After electrophoresis, gels were stained with silver using a Modified PlusOne Staining Kit (GE Healthcare Lifesciences) according to the manufacturer's instructions.

### **Covalent capture of thiophosphorylated peptides**

Thiophosphorylated peptides were isolated and converted to phosphopeptides for analysis by liquid chromatography–tandem mass spectrometry (LC-MS/MS) as described by Dingar *et al.* (3).

### **LC-MS/MS and data analysis**

Analysis of phosphopeptides was carried out by the Bio-Organic Biomedical Mass Spectrometry Resource at University of California, San Francisco (A.L.B.) by using a Linear Trap Quadrupole Orbitrap Velos electron transfer dissociation mass spectrometer (Thermo Fisher Scientific). Peptides were first separated by reverse-phase liquid chromatography using Eksigent nano 1D HPLC (Eksigent, Dublin, CA, USA) that was equipped with a 75 μm × 15 cm reverse-phase C-18 column (LC Packings; Conquer Scientific, San Diego, CA, USA). A 3–32% acetonitrile gradient in 0.1% formic acid was applied (350 nl/min flow rate) to separate peptides. LC-MS/MS was achieved by coupling the reverse-phase column with an atmospheric pressure ionization source in the mass spectrometer. Peptides were analyzed in positive ion mode. The 2 most intense multiple charged peaks from each mass spectrometry spectrum were selected for subsequent fragmentation with both collision-induced dissociation (CID) and electron transfer dissociation mechanisms to generate fragmentation spectra. MS/MS spectra were searched against the UniProt database by using Protein Prospector software to identify proteins and phospho sites.

### **LC-MS/MS of calpastatin Phostag**

Excised gel bands were washed in 100 mM NH<sub>4</sub>HCO<sub>3</sub> for 5 min before washing with acetonitrile for 5 min. Supernatant was removed, and gel pieces were rehydrated with additional acetonitrile. Acetonitrile was removed, and gel pieces were dehydrated by using a SpeedVac. Gel pieces were rehydrated by incubating with 10 mM DTT at 56°C for 30 min. Supernatant was removed and 2.5-min acetonitrile washes were repeated as before with subsequent gel dehydration by using a SpeedVac. Next, 55 mM iodoacetamide was added to the samples and incubated at room temperature for 20 min in the dark. Supernatant was discarded, and 2.5-min acetonitrile washes were carried out. For complete destaining of gels, gel pieces were incubated in a 1:1

solution of 100 mM  $\text{NH}_4\text{HCO}_3$  and acetonitrile at 37°C for 30 min. Supernatant was removed, and 2 5-min acetonitrile washes were carried out with subsequent gel dehydration by using a SpeedVac. Sufficient volume of 13 ng/ $\mu\text{l}$  trypsin in 50 mM  $\text{NH}_4\text{HCO}_3$  to cover gel pieces was added to samples and incubated at 4°C for 20 min. Unabsorbed trypsin was removed, and gel pieces were incubated with a minimal volume of 50 mM  $\text{NH}_4\text{HCO}_3$  to cover gel pieces. Samples were incubated at 37°C for 2 h, then overnight at room temperature. Gel pieces were washed with 50 mM  $\text{NH}_4\text{HCO}_3$  at 37°C for 5 min and washed with acetonitrile at 37°C for 10 min. Supernatants from washes were pooled together with a trypsin digest supernatant. Pooled samples were lyophilized by using a speed vacuum. Each sample was resuspended in 10  $\mu\text{l}$  of 50 mM  $\text{NH}_4\text{HCO}_3$  before LC-MS/MS analysis. Peptides were separated by reverse-phase LC using an EASY NanoLC system (Thermo Fisher Scientific) that was equipped with a 75- $\mu\text{m}$   $\times$  15-cm reverse-phase C-18 column. A 3-step linear gradient of acetonitrile in 0.1% formic acid was applied (300 nl/min flow rate over 180 min) to separate peptides. Eluent was ionized by electrospray ionization using an Orbitrap Velos Pro (Thermo Fisher Scientific) operating with Xcalibur software (v2.2; Thermo Fisher Scientific). Peptides were analyzed in positive ion mode. The instrument was programmed to acquire in automated data-dependent switching mode, selecting precursor ions on the basis of their intensity, for sequencing by CID fragmentation using a Top20 CID method. MS/MS analyses were conducted by using collision energy profiles that were chosen on the basis of the mass-to-charge ratio ( $m/z$ ) and the charge state of the peptide.

### Calpain activity assay

We measured calpain activity *in vitro* by using purified native calpain I from porcine erythrocytes (EMD Millipore, Billerica, MA, USA) in buffer that contained calcium (50 mM Tris HCl, pH 7.8, 30 mM NaCl, 1 mM DTT, and 3 mM CaCl) or buffer without calcium (50 mM Tris HCl, pH 7.8, 30 mM NaCl, 1 mM DTT, and 1 mM EGTA). All assays were in 100  $\mu\text{l}$  total volume in a 96-well format and carried out in triplicate. Each reaction contained 1  $\mu\text{g}$  of calpain I and 20  $\mu\text{M}$  of synthetic Suc-Leu-Leu-Val-Tyr-7-amino-4-methylcoumarin fluorescent substrate (Calbiochem, San Diego, CA, USA) in the appropriate buffer. Reactions were incubated for 10 min at 21°C before fluorescence readings were taken using the Gemini XS plate reader (Molecular Devices, San Jose, CA, USA) for 1 h. Fluorophores were excited at 380 nm and the emission of the cleaved substrate was measured at 460 nm.

### Data analysis

Data are presented as means  $\pm$  SD. Comparisons between groups were assessed for statistical significance by 1- or 2-way ANOVA or ANOVA with repeated measures, where applicable. Where significance was detected, individual mean values were compared by using Bonferroni's *post hoc* test.  $P$  values  $<0.05$  were considered statistically significant.

## RESULTS

### Estimation of p38 isoform expression in mouse heart

We first ascertained the relative level of expression of the 4 known p38 isoforms in WT mouse cardiac tissue. When GST-tagged active human recombinant p38 $\beta$ , p38 $\gamma$ , or

p38 $\delta$  MAPK (expected MW, 62 kDa) were added to crude heart homogenates and probed with Abs against each of these isoforms, we observed monoselective binding (Fig. 1A). Data suggest that there was little or no cross-reactivity between isoform-specific Abs. In addition, we used isoform-specific Abs against serially diluted (0.4–246 ng/0.05 mg total protein/well) recombinant p38 MAPK proteins to generate standard curves (data not shown) to determine the relative expression of each isoform in the murine heart (Fig. 1B). Our data suggest that the predominant isoforms that are expressed in the murine heart are p38 $\alpha$  and p38 $\gamma$ , which is in agreement with the literature (17). Confocal analysis of isolated mouse cardiac myocytes revealed that p38 MAPK—corresponding mainly to the p38 $\alpha$  MAPK isoform—is present in the cytoplasm and the nucleus (Fig. 1C). p38 $\beta$  MAPK is also localized in the cytoplasm and displays a striated pattern (Fig. 1D). p38 $\gamma$  presents a punctuate distribution in the cytoplasm of mouse cardiac myocytes (Fig. 1E) and, of interest, p38 $\delta$  expression was observed at the intercalated disks and the cytoplasm of cardiac myocytes (Fig. 1F). The selectivity of the signal was confirmed by using cardiac myocytes from p38 $\beta$ KO and p38 $\gamma$ / $\delta$ KO hearts and a negative control (no primary Ab).

### Mice that lack the p38 $\gamma$ isoform are protected against pressure overload hypertrophy

We observed that homozygous KO mice from the p38 $\gamma$  $\delta$ -targeted colony were resistant to cardiac hypertrophy when subjected to supra-renal aortic constriction (banding). WT hearts responded to both stressors by exhibiting a characteristic increase in heart mass (heart mass:body weight and heart weight:tibia length), systolic diameter, and end diastolic volume, as well as a decrease in ejection fraction (Fig. 2A–E). This effect was significantly blunted in p38 $\gamma$  $\delta$ KO mice for all relevant parameters. On the basis of the relative abundance of p38 $\gamma$  vs. p38 $\delta$  (Fig. 1), we hypothesized that this phenotype was the result of p38 $\gamma$  deficiency alone. After backcrossing, mice that lacked only the p38 $\gamma$  isoform demonstrated a response that was similar to those that lacked both p38 $\gamma$  and p38 $\delta$ . Of note, ejection fraction, fractional shortening, and endocardial fractional area of change were preserved in p38 $\gamma$ KO mice at 5 wk after banding (Fig. 3A–C) and KO hearts exhibited significantly less LV chamber dilatation and myocardial wall thickening compared with WT litter mates (Fig. 3D–F).

Consequently, hearts from p38 $\gamma$ KO mice were significantly smaller than those from WT mice (Fig. 4A), and there were fewer signs of pulmonary edema in KO mice as measured by the postmortem wet:dry weight of the lungs (Fig. 4B). Histochemical analysis of cryopreserved heart tissue revealed that p38 $\gamma$ KO hearts had less hypertrophic growth as shown by myocyte cross-sectional area (Fig. 4C) and myocardial expression of the slow isoform of myosin heavy chain ( $\beta$ -MHC) compared with WT littermates, which suggests that remodeling was reduced with the ablation of p38 $\gamma$  (Fig. 4D). We also observed the expression of p38 $\gamma$  in the nuclei of myocytes at 5 wk after banding (Fig. 4E), which is consistent with previous data (17).

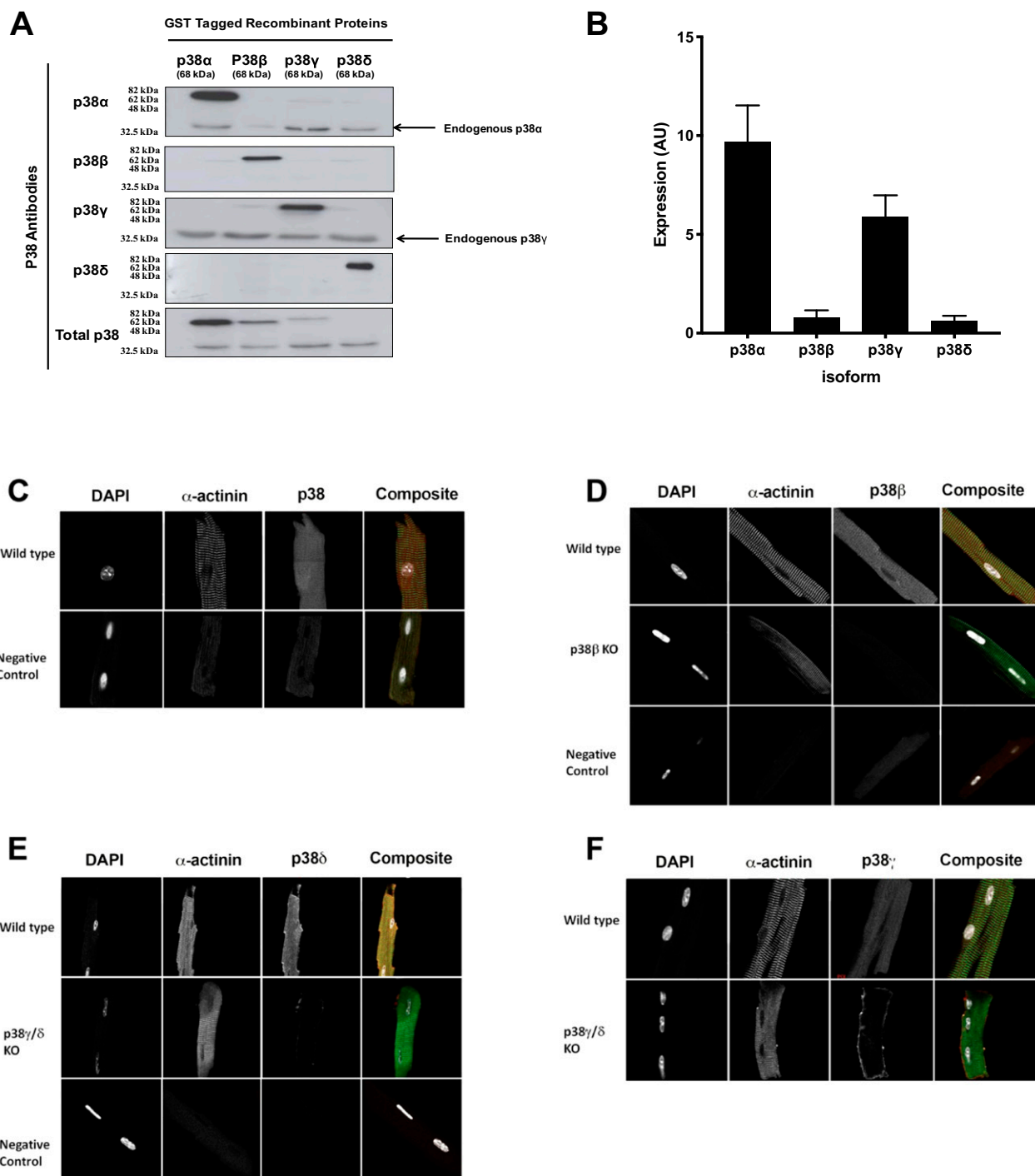


**Figure 1.** Characterization of p38 isoform expression in the mouse heart. Estimation of p38 isoforms in the mammalian heart. *A*) Whole-heart homogenates were spiked with GST-tagged recombinant proteins (240 ng/well) and probed with isoform-specific mAbs and a total (pan-isoform) Ab. Arrows indicate the endogenously expressed p38α and p38γ also detected in crude heart homogenate. *B*) After serial dilution of recombinant protein, standard curves were generated for each specific isoform Ab, and the relative endogenous expression of each isoform was determined. *C–F*) Expression and subcellular distribution of total Ab, corresponding mainly to p38α (*C*), p38β (*D*), p38γ (*E*), and p38δ MAPK (*F*) isoforms in isolated mouse cardiac myocytes. Negative control (*C–E*) contained no primary Ab. Data (*B*) are shown as means ± SD (*n* = 5/group).

### Nucleotide specificity of AS p38γ

To differentiate cardiac substrates of p38γ from other kinase substrates, we set out to identify an N<sup>6</sup> expanded ATP analog that could be utilized by AS p38γ, but not by WT p38γ, for phospho transfer. To achieve this, *in vitro* kinase

assays were set up using ATP and 4 different N<sup>6</sup> expanded ATP analogs [6-Bn-ATP, 6-PhEt-ATP, 6-Fu-ATP, and 6-(1-MeBu)-ATP]. AS p38γ could utilize all N<sup>6</sup> expanded ATP analogs tested to phosphorylate ATF2. In comparison, WT p38γ could not utilize the N<sup>6</sup> expanded ATP analogs to phosphorylate ATF2 as efficiently, as a signal for

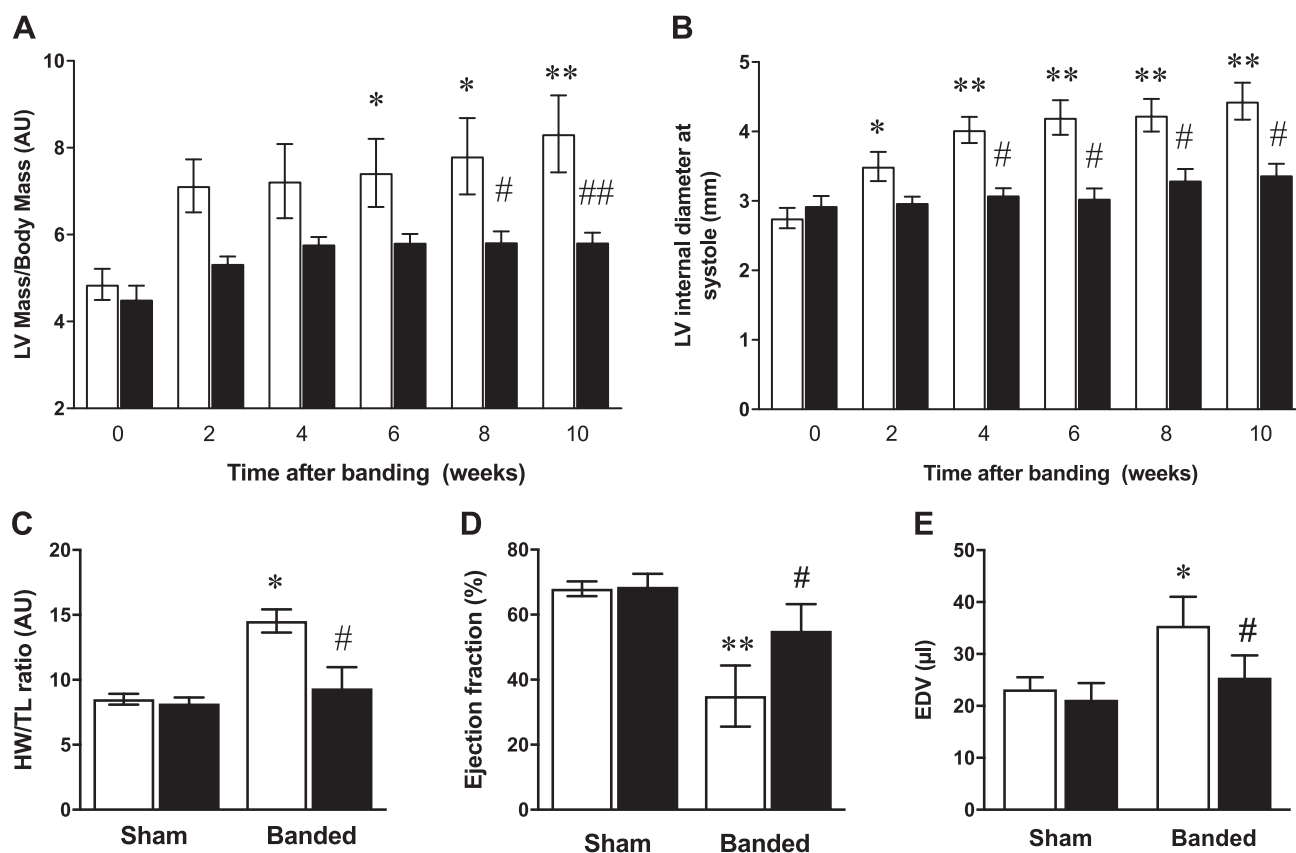


**Figure 2.** Physiologic and morphologic parameters measured in mice from WT and p38 $\gamma$ <sup>-/-</sup> $\delta$ <sup>-/-</sup> mice that were subjected to abdominal aortic banding surgery (banding). *A, B*) Calculated LV mass-to-body mass ratio (*A*) and LV end systolic diameter (*B*) in mice that were subjected to abdominal aortic banding assessed by serial cardiac ultrasound in WT (open bars) or p38 $\gamma$ / $\delta$  dual KO (black bars) mice. *C*) Heart weight (HW) -to-tibia length (TL) ratio assessed postmortem at 5 wk after banding surgery. *D, E*) Percent ejection fraction (*D*) and end diastolic volume (*E*) assessed by pressure-volume analysis at 5 wk after abdominal aortic banding. Data are shown as means  $\pm$  SD ( $n = 10$ –12/group). \* $P < 0.05$ , \*\* $P < 0.01$  vs. control; # $P < 0.05$ , ## $P < 0.01$  vs. corresponding WT control.

phosphorylated ATF2 was only observed with longer exposures (Fig. 5A, p-ATF2 probe, bottom). From this longer exposure, WT p38 $\gamma$  is less efficient at utilizing 6-PhEt-ATP and 6-(1-MeBu)-ATP than 6-Bn-ATP and 6-Fu-ATP. 6-PhEt-ATP was chosen for use in all subsequent experiments to label direct substrates of p38 $\gamma$ .

To specifically track and identify substrates of p38 $\gamma$  among the multitude of cardiac proteins, AS p38 $\gamma$  must be able to utilize 6-PhEt-ATP $\gamma$ S, which is further modified at the  $\gamma$ -phosphate to substitute a thiol group to thiophosphorylate downstream substrates (Fig. 5C). This was again assessed *in vitro* by using ATF2 as substrate (Fig. 5B). To detect thiophosphorylation of ATF2, kinase assays were subsequently alkylated with PNBM. This generates thiophosphate esters that form the epitope for recognition by the thiophosphate Ab. Whereas AS p38 $\gamma$  successfully thiophosphorylated ATF2 by using 6-PhEt-ATP $\gamma$ S, we did not observe thiophosphorylation of ATF2 with WT p38 $\gamma$  or in the nonalkylated AS p38 $\gamma$  control sample.

### Thiophosphorylation and identification of cardiac substrates by AS p38 $\gamma$

To identify cardiac substrates of p38 $\gamma$ , we incubated AS p38 $\gamma$  and 6-PhEt-ATP $\gamma$ S with WT murine heart

homogenate. Reactions were supplemented with 0.2 mM ATP and 3 mM GTP to reduce background signal caused by use of 6-PhEt-ATP $\gamma$ S by endogenous kinases (Supplemental Fig. 1). Upon termination of assays, a small sample of each assay was removed, alkylated with PNBM, and prepared for immunoblot analysis to monitor the thiophosphorylation reaction (Fig. 5D). Incubation of heart homogenate with both AS p38 $\gamma$  and 6-PhEt-ATP $\gamma$ S results in thiophosphorylation of many cardiac proteins. As thiophosphorylation was successfully determined, the remaining samples were processed in triplicate to enrich phosphopeptides and were analyzed by LC-MS/MS to identify substrates of p38 $\gamma$ . This identified 86 potential cardiac substrates of p38 $\gamma$  (Supplemental Table 1). Among the 86 proteins identified, LDB3 and calpastatin were identified as novel putative substrates of p38 $\gamma$ . LDB3 was determined to undergo phosphorylation at 2 potential sites (Ser<sup>98</sup> and Ser<sup>240</sup>), and calpastatin was determined to undergo phosphorylation at 6 potential sites (Thr<sup>216</sup>, Ser<sup>219</sup>, Ser<sup>459</sup>, Thr<sup>460</sup>, Ser<sup>466</sup>, and Thr<sup>467</sup>). Of interest, both LDB3 sites and 3 calpastatin sites (Thr<sup>216</sup>, Ser<sup>219</sup>, and Thr<sup>467</sup>) are adjacent to a +1 proline residue, which forms the consensus motif for MAPK phosphorylation.

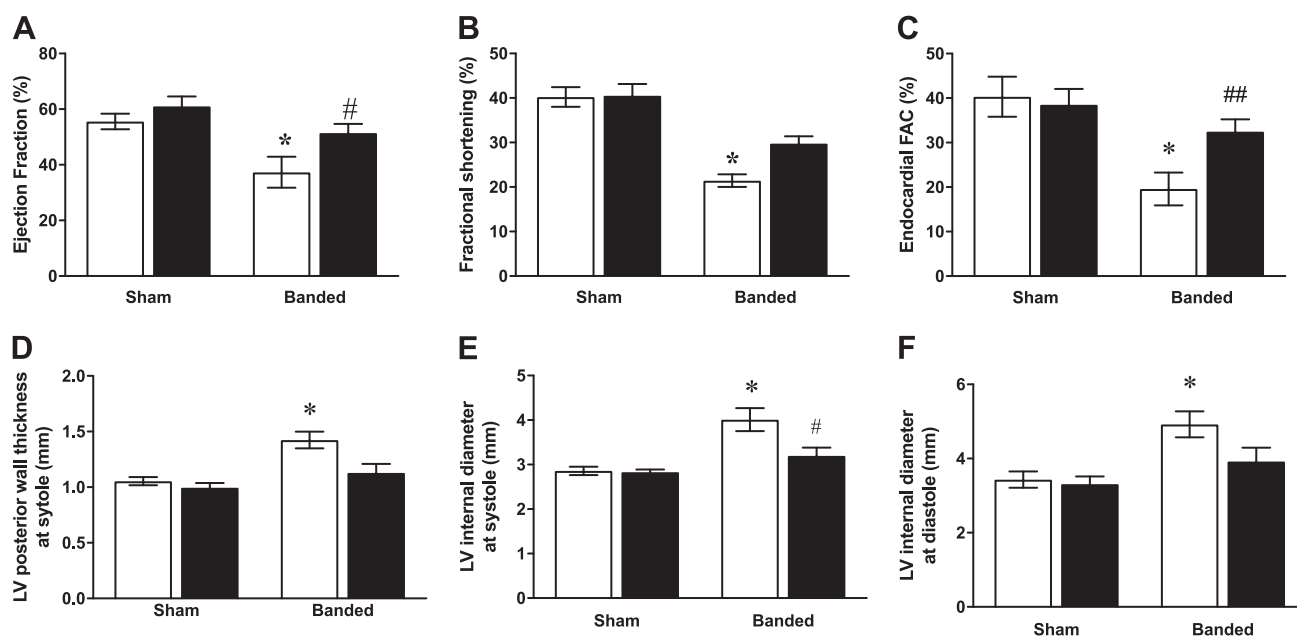


**Figure 3.** Ablation of p38 $\gamma$  protects mouse hearts from pathologic hypertrophy. Physiologic and morphologic parameters assessed by cardiac ultrasound in age- and sex-matched WT (open bars) and p38 $\gamma$ KO (black bars) mice at 5 wk after abdominal aortic banding (banded) or sham surgery. *A*) LV percent ejection fraction. *B*) LV fractional shortening. *C*) Endocardial fractional area changes (FAC%). *D*) LV posterior wall thickness at systole. *E*) LV internal diameter at systole. *F*) LV internal diameter at diastole. Data are shown as means  $\pm$  SD ( $n = 7$ – $9$ /group). \* $P < 0.05$  vs. control; # $P < 0.05$  and ## $P < 0.01$  vs. corresponding WT control.

### LDB3 and calpastatin are true substrates of p38 $\gamma$ *in vitro*

To validate LDB3 and calpastatin as true substrates of p38 $\gamma$ , we generated recombinant proteins for use in *in vitro* kinase assays with p38 $\gamma$ . To overcome the lack of phospho-specific Abs, kinase assays were performed with ATP $\gamma$ S and thiophosphorylation of proteins was examined. WT p38 $\gamma$  successfully thiophosphorylated LDB3 (Fig. 6A) and calpastatin (Fig. 7A). Stoichiometry of the phosphorylation of both substrates by WT p38 $\gamma$  using ATP was examined by Phostag SDS-PAGE gel and silver stain analysis. Phostag SDS-PAGE is a variation of the traditional SDS-PAGE analysis whereby the Phostag reagent captures phosphomonoester dianions that are bound to serine, threonine, or tyrosine residues and results in a mobility shift of the phosphorylated proteins in SDS-PAGE (16). In both cases, in contrast to control reactions, several higher MW bands were encountered upon LDB3 and calpastatin phosphorylation by p38 $\gamma$  (Figs. 6B and 7B, respectively). This is in agreement with the LC-MS/MS analysis that demonstrated that several sites are targeted for phosphorylation by p38 $\gamma$ . As LDB3 contains a PDZ domain, we investigated whether phosphorylation was PDZ interaction dependent by assessing LDB3 thiophosphorylation using WT and C-terminal truncated p38 $\gamma$ ; however, both WT and C'-truncated p38 $\gamma$  phosphorylated LDB3 to the same extent at all the time points measured.

As a positive control, we also examined the thiophosphorylation of  $\alpha$ 1-syntrophin, a known substrate of p38 $\gamma$  (5). As expected, WT p38 $\gamma$  successfully

thiophosphorylated  $\alpha$ 1-syntrophin (Fig. 6E). TAB1 is a substrate of p38 $\alpha$ , and we have previously shown that TAB1 interacts with p38 $\alpha$  *via* 2 distinct sites—at the upper canonical site used by other interacting partners of p38 $\alpha$  and a lower, noncanonical TAB1 unique binding site (16). As such, we investigated whether TAB1 is also phosphorylated by p38 $\gamma$  and included reactions with TAB1 mutated at the sites involved in canonical site interaction (CM). We found that, although p38 $\alpha$  enhances the phosphorylation of both WT and CM TAB1, as expected, p38 $\gamma$  was not able to phosphorylate TAB1 (Fig. 6D); therefore, TAB1 is not a substrate of p38 $\gamma$ .

We next sought to independently validate the p38 $\gamma$  phospho sites on calpastatin that were previously identified by LC-MS/MS analysis of thiophosphorylated cardiac proteins. For this, we excised bands from Phostag gels and performed LC-MS/MS analysis. This second round of analysis confirmed that all proline-directed sites that were initially detected (Ser<sup>98</sup> and Ser<sup>240</sup> for LDB3; Thr<sup>216</sup>, Ser<sup>219</sup>, and Thr<sup>467</sup> for calpastatin) are phosphorylated by p38 $\gamma$ . In addition, several other sites were determined to undergo phosphorylation by p38 $\gamma$  (Supplemental Tables 2 and 3). For subsequent experiments, we focused solely on the p38 $\gamma$ -mediated phosphorylation of calpastatin.

### Phosphorylation of Thr<sup>216</sup>, Ser<sup>219</sup>, and Thr<sup>467</sup> calpastatin by p38 $\gamma$

Calpastatin contains 4 repetitive inhibitory domains (I–IV) that can each reversibly inhibit 1 calpain molecule (18, 19).

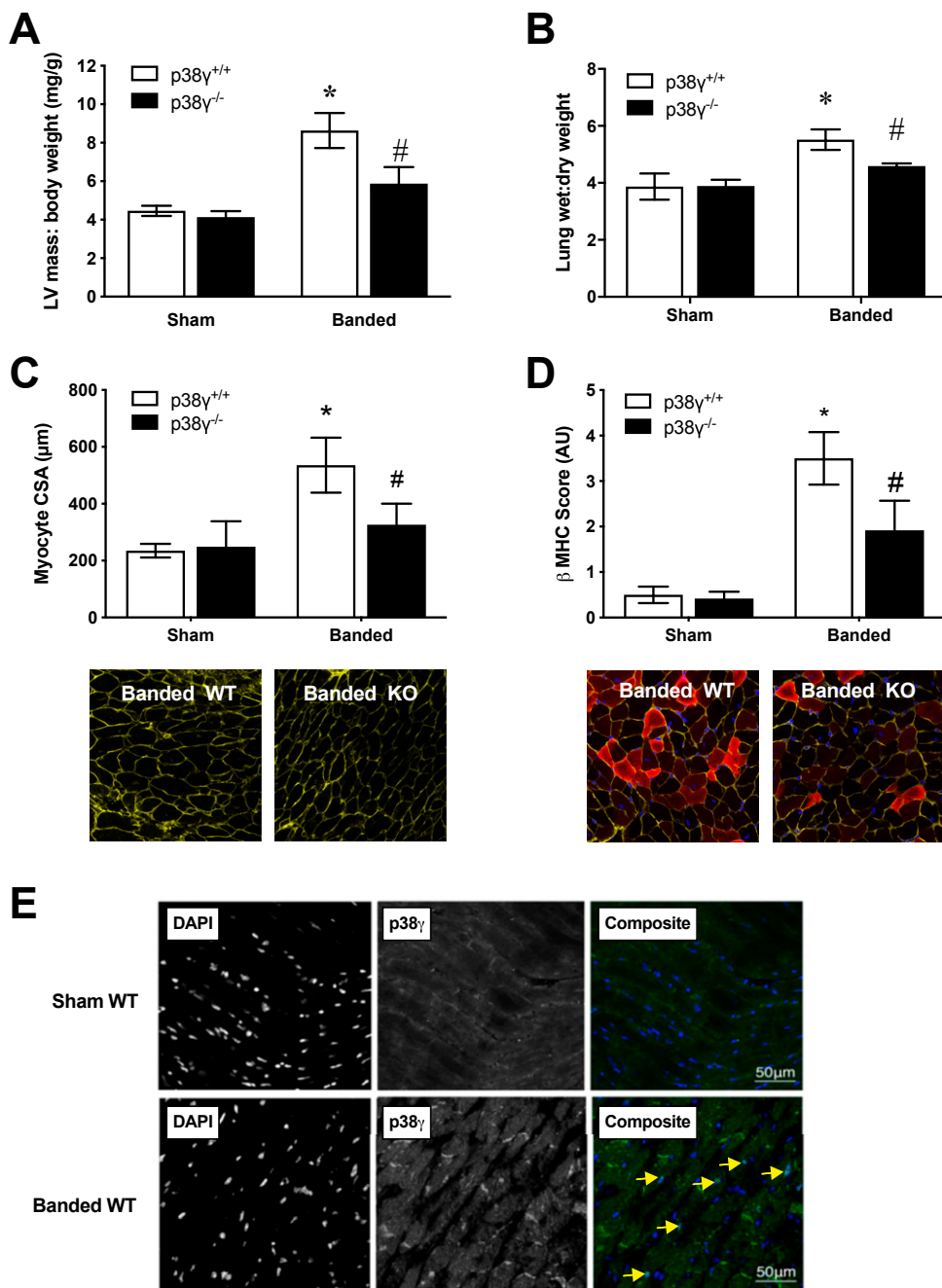


**Figure 4.** Ablation of p38 $\gamma$  protects mouse hearts from pathologic remodeling. Morphologic and histologic analysis of cardiac tissue from WT (open bars) and p38 $\gamma$ KO (black bars) mice at 5 wk after abdominal aortic banding (banded) or sham surgery. **A)** Calculated LV mass-to-body mass ratio. **B)** Lung wet-to-dry weight ratio was assessed postmortem. **C, D)** Myocyte cross-sectional area (**C**) and  $\beta$ -MHC expression (**D**) were assessed by confocal microscopy after cryo-sectioning at a thickness of 30  $\mu\text{m}$  and probing with the appropriate agents [anti- $\beta$ -MHC Ab and fluorophore-conjugated wheat germ agglutinin (WGA)] with computer-aided analysis. For each measure, a minimum of 5 images were used for measurements, and a minimum of 250 cells were analyzed from each heart. **E)** Subcellular localization of p38 $\gamma$  was determined by using specific Abs in sham and banded (5 wk) hearts. Arrows indicate localization of p38 $\gamma$  immunoreactivity in nuclei of cardiac myocytes. Data are shown as means  $\pm$  SD ( $n = 7$ –9/group). \* $P < 0.05$  vs. control, # $P < 0.05$  vs. corresponding WT control.

Examination of the peptide sequence and crystal structure of calpastatin revealed that Thr<sup>216</sup> and Ser<sup>219</sup> are located before the first inhibitory domain of calpastatin, and Thr<sup>467</sup> is located between inhibitory domains II and III. Therefore, we engineered double T216A/S219A- and a single T467A phosphorylation-deficient mutants of calpastatin. As before, purified mutants were subject to *in vitro* kinase assays with p38 $\gamma$  and ATP (Fig. 7C). Samples were then probed with custom calpastatin phospho-Abs against these sites. Both phospho-calpastatin Abs—pT216/S216 and pT467—detected phosphorylation of WT calpastatin, but not of the respective alanine mutants, which confirmed that Thr<sup>216</sup>, Ser<sup>219</sup>, and Thr<sup>467</sup> are phosphorylated by p38 $\gamma$  *in vitro*.

### Phosphorylation of calpastatin reduces its inhibitory efficiency

To determine what effect phosphorylation has on the function of calpastatin, we next conducted *in vitro* fluorometric calpain assays. The synthetic calpain substrate, 7-amino-5-methylcoumarin, is cleaved by calpain, which results in increased fluorescence only when calcium is present in the buffer (Fig. 8A). The addition of recombinant WT calpastatin (0.2–4.5  $\mu\text{g}$ ) to the assay in its non-phosphorylated form resulted in the dose-dependent inhibition of calpain activity, as a corresponding decrease in fluorescence was observed (Fig. 8B). Lastly, a significant difference was observed in the inhibition of calpain by

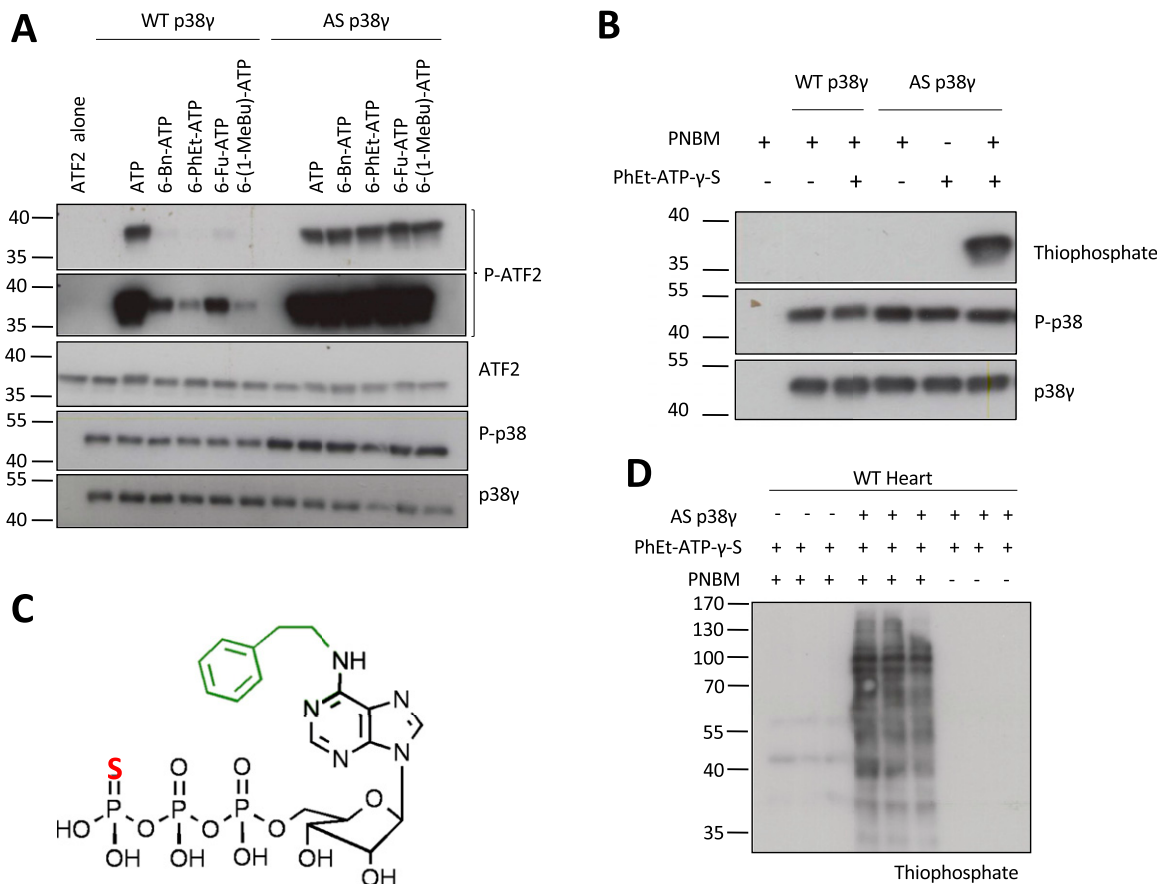


**Figure 5.** Immunoblot analysis of *in vitro* kinase assays of p38 $\gamma$  kinases with ATF2 or WT heart homogenate as substrate. **A**) Phosphorylation of ATF2 (1  $\mu$ g) by WT and AS p38 $\gamma$  kinases (200 ng) using ATP (1 mM) and various N<sup>6</sup> expanded ATP analogs (1 mM) after 30 min at 30°C. For the phospho-ATF2 signal, 2 different exposures of film are shown. **B**) Thiophosphorylation of ATF2 by WT and AS p38 $\gamma$  kinases using PhEt-ATP- $\gamma$ -S (1 mM). Samples were alkylated with PNBM (5 mM) for 1 h before immunoblot analysis. **C**) Chemical structure of PhEt-ATP- $\gamma$ -S. **D**) Thiophosphorylation of cardiac proteins after spiking of WT heart homogenate (2 mg) with recombinant AS p38 $\gamma$  (20  $\mu$ g) and 6-PhEt-ATP $\gamma$ S (1 mM) in triplicate. A 20- $\mu$ l aliquot was removed from each reaction and alkylated with PNBM (5 mM) for 1 h before immunoblot analysis. Remaining samples were processed for LC-MS/MS.

calpastatin between its nonphosphorylated and p38 $\gamma$ -phosphorylated form (Fig. 8C). Increased fluorescence was observed with phospho-calpastatin, which indicated that phosphorylation of calpastatin by p38 $\gamma$  reduces the inhibitory efficiency of calpastatin. This reduction of the inhibitory effect of calpastatin was reversed when we used a double T216A/S219A phosphorylation-deficient mutant of calpastatin (Fig. 8C)

## DISCUSSION

The purpose of the current study was to decipher the role played by p38 $\gamma$  in the heart. To summarize our findings, we have shown that p38 $\gamma$  is expressed in the heart and is an important regulator of the progression of cardiac hypertrophy. By using the Shokat approach to identify substrates of protein kinases, we have discovered LDB3 and calpastatin, among other substrates, to be novel targets of p38 $\gamma$ . Both proteins are indispensable to cardiac myocyte function. LDB3 is a key cytoskeletal protein in cardiomyocytes, and calpastatin is the natural and endogenous inhibitor of calpain proteases. Although we were

unable to assess the consequences of p38 $\gamma$ -mediated LDB3 phosphorylation, we observed that phosphorylation of calpastatin by p38 $\gamma$  reduces the efficiency of calpastatin in inhibiting calpain. If this disinhibition occurs *in vivo*, it may be an important mechanism by which p38 $\gamma$  mediates its prohypertrophic role in the heart.

## Phenotype of p38 $\gamma$ KO mice after cardiac stress

Data presented here confirm the prohypertrophic role of p38 $\gamma$  in the myocardium. Global p38 $\gamma$ KO mice are less susceptible to the effects of pressure overload hypertrophy compared with WT controls (Figs. 2 and 3), which is consistent with the recent findings by the Sabio group (9). The LV of WT mice gradually increased in mass and contraction was impaired, as indicated by an increase in internal diameter. Despite the roles for this isoform that have been described in skeletal muscle development and maintenance, blunted growth of p38 $\gamma$ KO mice was not a confounding factor in this study (20).

Immunohistochemistry of hearts revealed an increase in the expression of  $\beta$ -MHC and an increase in myocyte

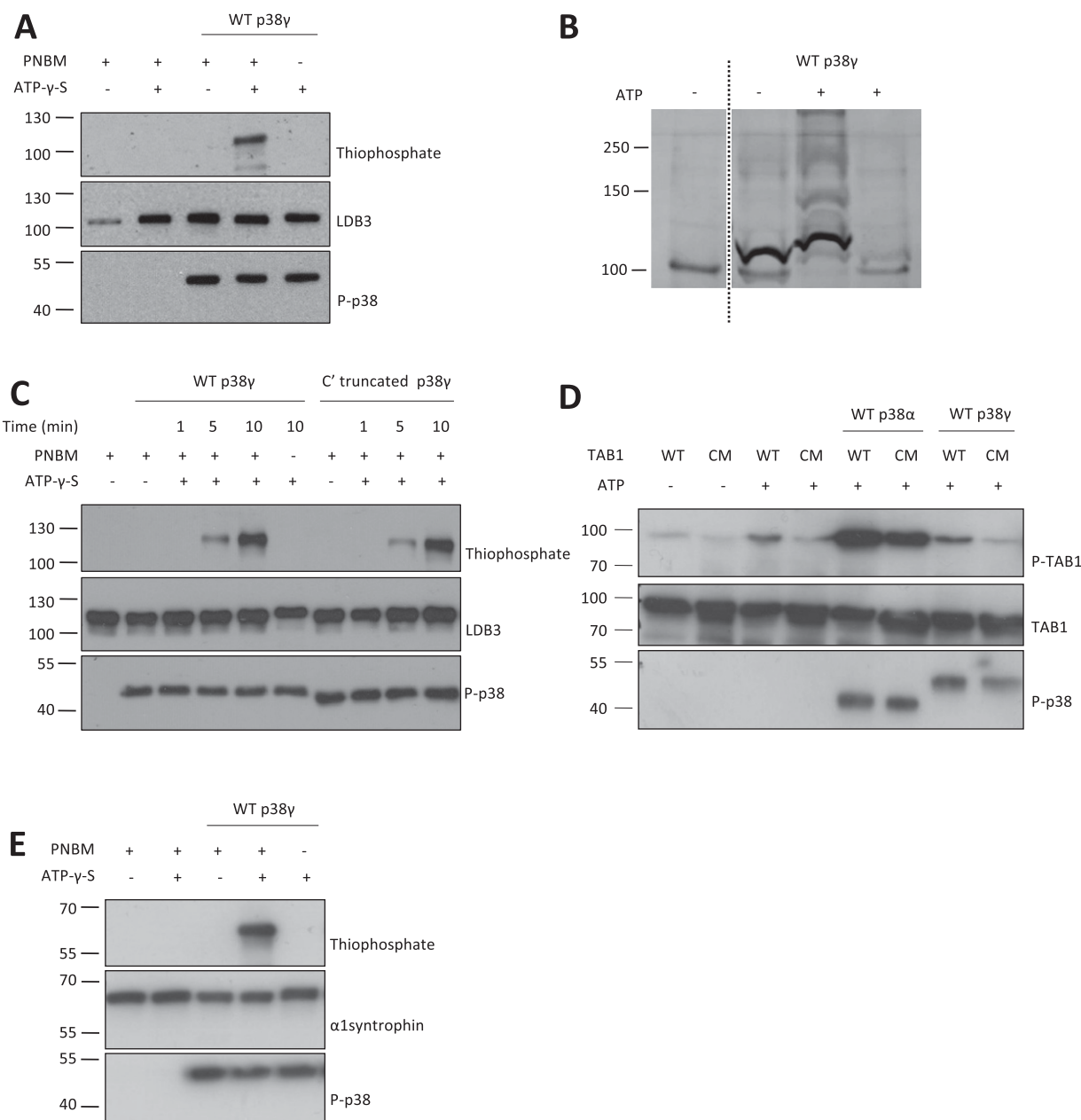


**Figure 6.** *In vitro* validation of LDB3 and  $\alpha$ 1-syntrophin, but not TAB1, as substrates of p38 $\gamma$ . **A**) Immunoblot analysis of LDB3 (1  $\mu$ g) thiophosphorylation by WT p38 $\gamma$  (200 ng) using ATP $\gamma$ S (1 mM) after 30 min at 30°C. **B**) Phostag SDS-PAGE gel and silver stain analysis of LDB3 phosphorylation by WT p38 $\gamma$  with ATP (1 mM) after 30 min at 30°C (dotted line indicates where irrelevant lanes have been removed for clarity). **C**) Immunoblot analysis of LDB3 (1  $\mu$ g) thiophosphorylation by WT or C' truncated p38 $\gamma$  (200 ng) using ATP $\gamma$ S after 1, 5, or 10 min. **D**) Immunoblot analysis of WT TAB1 or CM TAB1 phosphorylation by WT p38 $\alpha$  and p38 $\gamma$  with ATP after 30 min at 30°C. **E**) Immunoblot analysis of  $\alpha$ 1-syntrophin (1  $\mu$ g) thiophosphorylation by WT p38 $\gamma$  using ATP $\gamma$ S after 30 min at 30°C.

cross-sectional area, both of which are hallmarks of experimental cardiac hypertrophy (5, 21, 22), in banded WT but not KO hearts (Fig. 3), which supports the observation that p38 $\gamma$  is involved in the progression of pathologic cardiac hypertrophy.

### Cardiac substrates of p38 $\gamma$

Two novel cardiac substrates of p38 $\gamma$  identified in the current study are LDB3 and calpastatin. Extensive characterization of these proteins and their p38 $\gamma$  phosphorylation

sites has been carried out *in vitro*, and we have confirmed the phosphorylation of both proteins by p38 $\gamma$  (Figs. 6 and 7). Phostag gel analysis, mass spectrometry, and custom phospho-Abs against the phosphorylated protein substrates demonstrate that both substrates are phosphorylated by p38 $\gamma$  at multiple sites. LDB3 is phosphorylated by p38 $\gamma$  at Ser<sup>98</sup> and Ser<sup>240</sup>, and calpastatin is phosphorylated by p38 $\gamma$  at Thr<sup>197</sup>/Ser<sup>200</sup> and Thr<sup>448</sup> (Fig. 7). All sites, to our knowledge, are novel phosphorylation sites that have not previously been described. Of interest, both substrates identified here have previously been implicated in cardiac hypertrophy, as discussed further below.

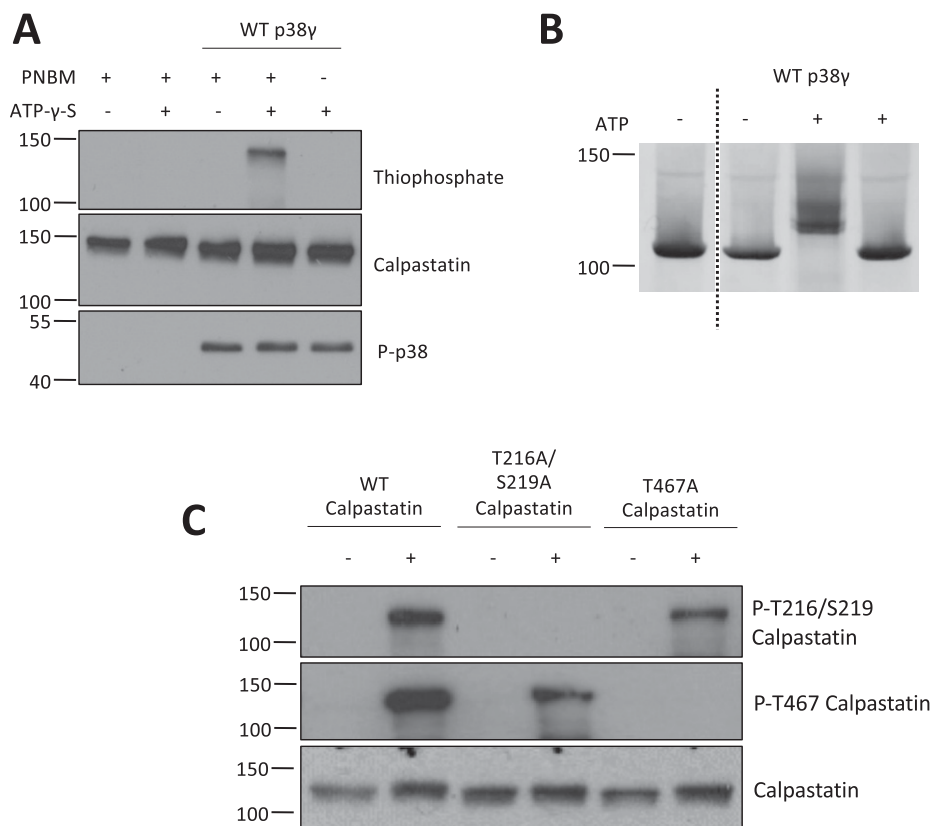


**Figure 7.** *In vitro* validation of calpastatin (CS) as a substrate of p38 $\gamma$ , and determination of CS residues Thr<sup>216</sup> and/or Ser<sup>219</sup> and Thr<sup>467</sup> as targets of p38 $\gamma$ . **A**) Immunoblot analysis of CS (1  $\mu$ g) thio-phosphorylation by WT p38 $\gamma$  (200 ng) using ATP $\gamma$ S (1 mM) after 30 min at 30°C. **B**) Phostag SDS-PAGE gel and silver stain analysis of CS phosphorylation by WT p38 $\gamma$  with ATP (1 mM) after 30 min at 30°C (dotted line indicates where irrelevant lanes have been removed for clarity). **C**) Immunoblot analysis of WT and phospho-mutant CS phosphorylation by WT p38 $\gamma$  with ATP after 30 min at 30°C

### LDB3

LDB3 is a key cytoskeletal scaffold protein in cardiomyocytes (23). LDB3-null mice are not viable, and cardiac-specific or inducible cardiac-specific LDB3 KO mice display disrupted cardiomyocyte structure, decreased cardiac function, and eventually develop a severe form of dilated cardiomyopathy, followed by premature death (24). Furthermore, mutations in the *ZASP* gene (human ortholog) have been associated with dilated cardiomyopathies (25) and LV noncompaction (25, 26) in humans, which demonstrates the essential role of LDB3 in the heart.

Of interest, LDB3 contains a PDZ domain; however, the interaction of the PDZ domain of LDB3 with the PDZ domain-interacting motif of p38 $\gamma$  was not necessary for successful substrate phosphorylation, as C' truncated p38 $\gamma$  could phosphorylate LDB3 to the same extent as WT p38 $\gamma$ , at least under *in vitro* experimental conditions tested here (Fig. 6).

### Calpastatin

Calpastatin is the natural and endogenous inhibitor of calpain proteases. Calpain proteases are cysteine-dependent proteases that are activated by increased intracellular calcium in such scenarios as cardiac hypertrophy and remodeling. Previous studies have demonstrated that inhibition of calpain activity during pathophysiological circumstances demonstrates favorable

improvements in cardiac function (27–29). Results from animal studies of calpain in cardiac remodeling are supported by data from patients with congestive heart failure. A significant increase in calpain 1 and 2 protein and a concomitant increase in the cleavage of calpain substrate cain/cabin 1 has been reported in severe failing hearts compared with hearts from healthy controls (30).

In support of previous studies (31, 32), we have clearly demonstrated that phospho modification of calpastatin can modulate its ability to inhibit calpain. We speculate that this may be a mechanism by which p38 $\gamma$  mediates its prohypertrophic role in the heart. A crucial substrate of calpain is the serine/threonine-specific phosphatase, calcineurin. Elevation in intracellular calcium or cleavage of the autoinhibitory domain of calcineurin by calpain can activate calcineurin (33). Once active, calcineurin dephosphorylates nuclear factor of activated T cell (NFAT) transcription factors, key prohypertrophic transcription factors in the heart. Dephosphorylated NFAT transcription factors then translocate to the nucleus to increase transcription of prohypertrophic genes. In principle, this could place p38 $\gamma$  within a well-established hypertrophic signaling cascade. p38 $\gamma$ -mediated phosphorylation of calpastatin would result in unrestrained calpain activity, increased calcineurin activation, and a concomitant increase in NFAT activity. Although other targets of p38 $\gamma$  may contribute to the development of pathologic cardiac hypertrophy, this pathway may explain, in part, the resistance of p38 $\gamma$ KO mice to

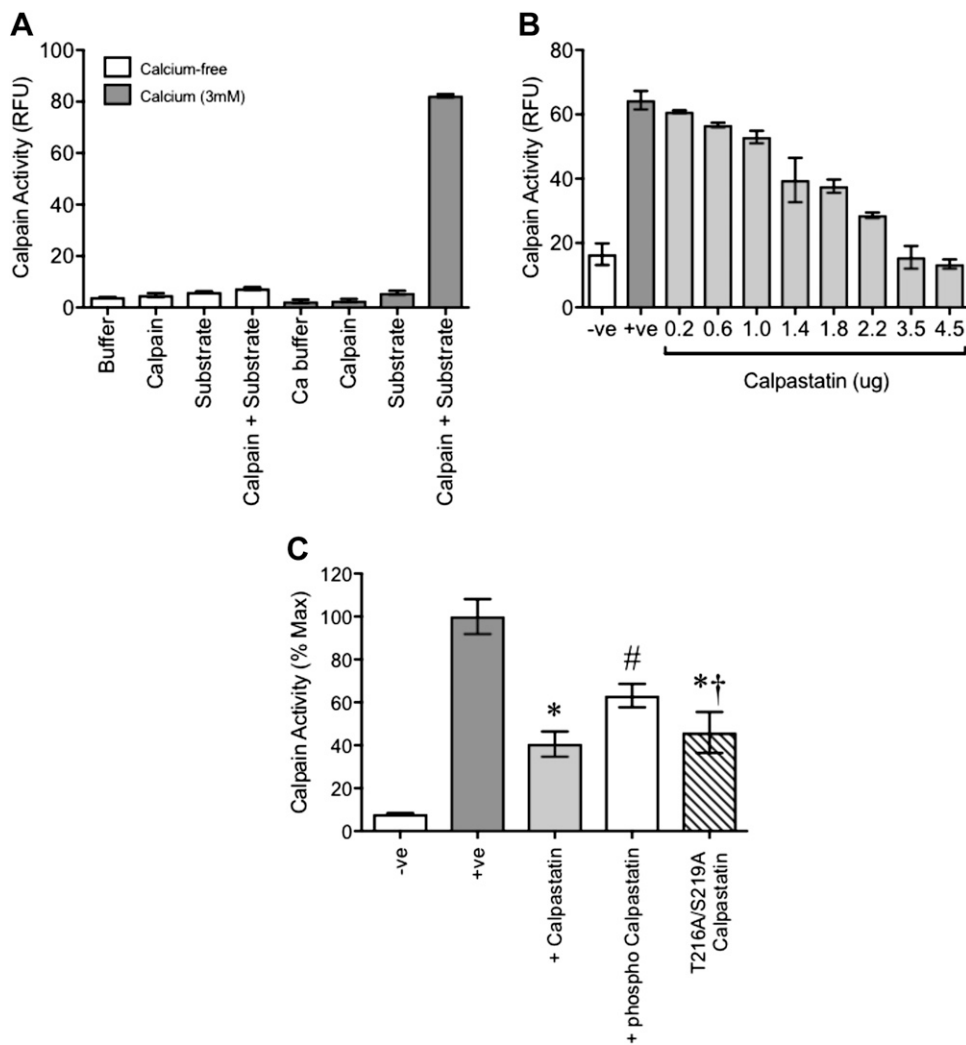


**Figure 8.** Phosphorylation of calpastatin by p38 $\gamma$  reduces its ability to inhibit calpain *in vitro*. Cleavage of the synthetic peptide substrate, Suc-Leu-Leu-Val-Try-AMC (amino-4-methylcoumarin; 20  $\mu$ M), by calpain (1  $\mu$ g) liberates the AMC fluorophore. **A)** Fluorescence or calpain activity is only observed in the presence of 1 mM calcium. **B)** Dose-dependent inhibition of calpain by calpastatin (0.2–4.5  $\mu$ g). **C)** Calpain activity (normalized to percentage of maximal activity) in the presence of WT calpastatin (1.8  $\mu$ g), phosphorylated calpastatin, and T216A/S219A phosphor-dead mutant calpastatin. Data are shown as means  $\pm$  SEM ( $n = 3$ ). \* $P < 0.05$  vs. calpain activity positive control, # $P < 0.05$  vs. calpain activity with nonphosphorylated calpastatin, † $P < 0.05$  vs. phosphorylated WT calpastatin.

pressure overload hypertrophy compared with WT mice and warrants additional investigation. **FJ**

supported by NIH NIGMS Grant 8P41-GM103481 and Howard Hughes Medical Institute. The authors declare no conflicts of interest.

## ACKNOWLEDGMENTS

This work was supported by the Department of Health *via* the National Institute for Health Research Comprehensive Biomedical Research Centre and Clinical Research Facilities awards to Guy and St. Thomas National Health Service (NHS) Foundation Trust, in partnership with King's College London and King's College Hospital NHS Foundation Trust. A.A.L. was funded by King's College London Graduate School. N.S.-S. was funded by the British Heart Foundation. E.D.M. was funded by British Heart Foundation (SP/14/2/30922) and Medical Research Council (MR/J007501/1). P.A. was funded by Biotechnology and Biological Sciences Research Council CASE Ph.D. studentship award with GlaxoSmithKline (STU100019047). This research was supported by the British Heart Foundation (SP/14/2/30922), Medical Research Council (MR/J007501/1), and Graduate School of King's College London. Mass spectrometry data was provided by the Bio-Organic Biomedical Mass Spectrometry Resource at University of California–San Francisco (to A.L.B.), supported by the Biomedical Technology Research Centers Program of the U.S. National Institutes of Health (NIH) National Institute of General Medical Sciences (NIGMS); and the Thermo Fisher Scientific Linear Trap Quadrupole Orbitrap Velos,

## AUTHOR CONTRIBUTIONS

A. A. Loonat, M. S. Marber, and J. E. Clark designed research; A. A. Loonat, N. Sarafraz-Shakary, K. Tilgner, S. Uddin, M. Thomas, and J. E. Clark performed *in vivo* experiments and analyzed data; A. A. Loonat and E. D. Martin performed *in vitro* research; A. A. Loonat, M. S. Marber, and J. E. Clark wrote the manuscript; and N. T. Hertz, R. Levin, K. M. Shokat, and A. L. Burlingame contributed new reagents or analytic tools.

## REFERENCES

- Denise Martin, E., De Nicola, G. F., and Marber, M. S. (2012) New therapeutic targets in cardiology: p38 alpha mitogen-activated protein kinase for ischemic heart disease. *Circulation* **126**, 357–368
- Kumar, S., McDonnell, P. C., Gum, R. J., Hand, A. T., Lee, J. C., and Young, P. R. (1997) Novel homologues of CSBP/p38 MAP kinase: activation, substrate specificity and sensitivity to inhibition by pyridinyl imidazoles. *Biochem. Biophys. Res. Commun.* **235**, 533–538

3. Dingar, D., Merlen, C., Grandy, S., Gillis, M. A., Villeneuve, L. R., Mamarbachi, A. M., Fiset, C., and Allen, B. G. (2010) Effect of pressure overload-induced hypertrophy on the expression and localization of p38 MAP kinase isoforms in the mouse heart. *Cell. Signal.* **22**, 1634–1644
4. Court, N. W., dos Remedios, C. G., Cordell, J., and Bogoyevitch, M. A. (2002) Cardiac expression and subcellular localization of the p38 mitogen-activated protein kinase member, stress-activated protein kinase-3 (SAPK3). *J. Mol. Cell. Cardiol.* **34**, 413–426
5. Hasegawa, M., Cuenda, A., Spillantini, M. G., Thomas, G. M., Buée-Scherrer, V., Cohen, P., and Goedert, M. (1999) Stress-activated protein kinase-3 interacts with the PDZ domain of alpha1-syntrophin. A mechanism for specific substrate recognition. *J. Biol. Chem.* **274**, 12626–12631
6. Sabio, G., Reuver, S., Feijoo, C., Hasegawa, M., Thomas, G. M., Centeno, F., Kuhlendahl, S., Leal-Ortiz, S., Goedert, M., Garner, C., and Cuenda, A. (2004) Stress- and mitogen-induced phosphorylation of the synapse-associated protein SAP90/PSD-95 by activation of SAPK3/p38gamma and ERK1/ERK2. *Biochem. J.* **380**, 19–30
7. Sabio, G., Arthur, J. S., Kuma, Y., Pegg, M., Carr, J., Murray-Tait, V., Centeno, F., Goedert, M., Morrice, N. A., and Cuenda, A. (2005) p38gamma regulates the localisation of SAP97 in the cytoskeleton by modulating its interaction with GKAP. *EMBO J.* **24**, 1134–1145
8. Hou, S. W., Zhi, H. Y., Pohl, N., Loesch, M., Qi, X. M., Li, R. S., Basir, Z., and Chen, G. (2010) PTPH1 dephosphorylates and cooperates with p38gamma MAPK to increase Ras oncogenesis through PDZ-mediated interaction. *Cancer Res.* **70**, 2901–2910
9. González-Terán, B., López, J. A., Rodríguez, E., Leiva, L., Martínez-Martínez, S., Bernal, J. A., Jiménez-Borreguero, L. J., Redondo, J. M., Vazquez, J., and Sabio, G. (2016) p38γ and δ promote heart hypertrophy by targeting the mTOR-inhibitory protein DEPTOR for degradation. *Nat. Commun.* **7**, 10477
10. Shah, K., Liu, Y., Deirmengian, C., and Shokat, K. M. (1997) Engineering unnatural nucleotide specificity for Rous sarcoma virus tyrosine kinase to uniquely label its direct substrates. *Proc. Natl. Acad. Sci. USA* **94**, 3565–3570
11. Allen, J. J., Li, M., Brinkworth, C. S., Paulson, J. L., Wang, D., Hübner, A., Chou, W. H., Davis, R. J., Burlingame, A. L., Messing, R. O., Katayama, C. D., Hedrick, S. M., and Shokat, K. M. (2007) A semisynthetic epitope for kinase substrates. *Nat. Methods* **4**, 511–516
12. Boguslavskyi, A., Pavlovic, D., Aughton, K., Clark, J. E., Howie, J., Fuller, W., and Shattock, M. J. (2014) Cardiac hypertrophy in mice expressing unphosphorylatable phospholemman. *Cardiovasc. Res.* **104**, 72–82
13. Clark, J. E., and Marber, M. S. (2013) Advancements in pressure-volume catheter technology—stress remodelling after infarction. *Exp. Physiol.* **98**, 614–621
14. Haworth, R. S., McCann, C., Snabaitis, A. K., Roberts, N. A., and Avkiran, M. (2003) Stimulation of the plasma membrane Na<sup>+</sup>/H<sup>+</sup> exchanger NHE1 by sustained intracellular acidosis. Evidence for a novel mechanism mediated by the ERK pathway. *J. Biol. Chem.* **278**, 31676–31684
15. Gillespie, M. A., Le Grand, F., Scimè, A., Kuang, S., von Maltzahn, J., Seale, V., Cuenda, A., Ranish, J. A., and Rudnicki, M. A. (2009) p38-gamma-dependent gene silencing restricts entry into the myogenic differentiation program. *J. Cell Biol.* **187**, 991–1005
16. DeNicola, G. F., Martin, E. D., Chaikuad, A., Bassi, R., Clark, J., Martino, L., Verma, S., Sicard, P., Tata, R., Atkinson, R. A., Knapp, S., Conte, M. R., and Marber, M. S. (2013) Mechanism and consequence of the autoactivation of p38α mitogen-activated protein kinase promoted by TAB1. *Nat. Struct. Mol. Biol.* **20**, 1182–1190
17. Hertz, N. T., Wang, B. T., Allen, J. J., Zhang, C., Dar, A. C., Burlingame, A. L., and Shokat, K. M. (2010) Chemical genetic approach for kinase-substrate mapping by covalent capture of thiophosphopeptides and analysis by mass spectrometry. *Curr. Protoc. Chem. Biol.* **2**, 15–36
18. Moldoveanu, T., Gehring, K., and Green, D. R. (2008) Concerted multi-pronged attack by calpastatin to occlude the catalytic cleft of heterodimeric calpains. *Nature* **456**, 404–408
19. Hanna, R. A., Campbell, R. L., and Davies, P. L. (2008) Calcium-bound structure of calpain and its mechanism of inhibition by calpastatin. *Nature* **456**, 409–412
20. Foster, W. H., Tidball, J. G., and Wang, Y. (2012) p38γ activity is required for maintenance of slow skeletal muscle size. *Muscle Nerve* **45**, 266–273
21. Kehat, I., and Molkentin, J. D. (2010) Molecular pathways underlying cardiac remodeling during pathophysiological stimulation. *Circulation* **122**, 2727–2735
22. Barry, S. P., Davidson, S. M., and Townsend, P. A. (2008) Molecular regulation of cardiac hypertrophy. *Int. J. Biochem. Cell Biol.* **40**, 2023–2039
23. Hoshijima, M. (2006) Mechanical stress-strain sensors embedded in cardiac cytoskeleton: Z disk, titin, and associated structures. *Am. J. Physiol. Heart Circ. Physiol.* **290**, H1313–H1325
24. Zheng, M., Cheng, H., Li, X., Zhang, J., Cui, L., Ouyang, K., Han, L., Zhao, T., Gu, Y., Dalton, N. D., Bang, M. L., Peterson, K. L., and Chen, J. (2009) Cardiac-specific ablation of Cypher leads to a severe form of dilated cardiomyopathy with premature death. *Hum. Mol. Genet.* **18**, 701–713
25. Lopez-Ayala, J. M., Ortiz-Genga, M., Gomez-Milanes, I., Lopez-Cuenca, D., Ruiz-Espejo, F., Sanchez-Munoz, J. J., Oliva-Sandoval, M. J., Monserrat, L., and Gimeno, J. R. (2015) A mutation in the Z-line Cypher/ZASP protein is associated with arrhythmogenic right ventricular cardiomyopathy. *Clin. Genet.* **88**, 172–176
26. Vatta, M., Mohapatra, B., Jimenez, S., Sanchez, X., Faulkner, G., Perles, Z., Sinagra, G., Lin, J. H., Vu, T. M., Zhou, Q., Bowles, K. R., Di Lenarda, A., Schimmenti, L., Fox, M., Chrisco, M. A., Murphy, R. T., McKenna, W., Elliott, P., Bowles, N. E., Chen, J., Valle, G., and Towbin, J. A. (2003) Mutations in Cypher/ZASP in patients with dilated cardiomyopathy and left ventricular non-compaction. *J. Am. Coll. Cardiol.* **42**, 2014–2027
27. Letavernier, E., Perez, J., Bellocq, A., Mesnard, L., de Castro Keller, A., Haymann, J. P., and Baud, L. (2008) Targeting the calpain/calpastatin system as a new strategy to prevent cardiovascular remodeling in angiotensin II-induced hypertension. *Circ. Res.* **102**, 720–728
28. Li, Y., Ma, J., Zhu, H., Singh, M., Hill, D., Greer, P. A., Arnold, J. M., Abel, E. D., and Peng, T. (2011) Targeted inhibition of calpain reduces myocardial hypertrophy and fibrosis in mouse models of type 1 diabetes. *Diabetes* **60**, 2985–2994
29. Ye, T., Wang, Q., Zhang, Y., Song, X., Yang, D., Li, D., Li, D., Su, L., Yang, Y., and Ma, S. (2015) Over-expression of calpastatin inhibits calpain activation and attenuates post-infarction myocardial remodeling. *PLoS One* **10**, e0120178
30. Yang, D., Ma, S., Tan, Y., Li, D., Tang, B., Zhang, X., Sun, M., and Yang, Y. (2010) Increased expression of calpain and elevated activity of calcineurin in the myocardium of patients with congestive heart failure. *Int. J. Mol. Med.* **26**, 159–164
31. Salamino, F., Averna, M., Tedesco, I., De Tullio, R., Melloni, E., and Pontremoli, S. (1997) Modulation of rat brain calpastatin efficiency by post-translational modifications. *FEBS Lett.* **412**, 433–438
32. Averna, M., De Tullio, R., Salamino, F., Melloni, E., and Pontremoli, S. (1999) Phosphorylation of rat brain calpastatins by protein kinase C. *FEBS Lett.* **450**, 13–16
33. Burkard, N., Becher, J., Heindl, C., Neyses, L., Schuh, K., and Ritter, O. (2005) Targeted proteolysis sustains calcineurin activation. *Circulation* **111**, 1045–1053

Received for publication December 21, 2017.

Accepted for publication March 26, 2018.